Hawaiian Regional Climate Variability during Two Types of El Niño

BO-YI LU,[a] PAO-SHIN CHU,[a] SUNG-HUN KIM,[a] AND CHRISTINA KARAMPERIDOU[a]

[a] *Department of Atmospheric Sciences, School of Ocean and Earth Science and Technology, University of Hawaiʻi at Mānoa, Honolulu, Hawaii*

ABSTRACT: The large-scale atmospheric circulation of the North Pacific associated with two types of El Niño—the eastern Pacific (EP) and central Pacific (CP)—is studied in relation to Hawaiian winter (December–February) rainfall and temperature. The eastern and central equatorial Pacific undergo active convective heating during EP El Niño winters. The local Hadley circulation is enhanced and an upper-level westerly jet stream of the North Pacific is elongated eastward. Due to the impact of both phenomena, stronger anomalous descending motion, moisture flux divergence anomalies near Hawaii, and reduction of easterly trade winds, which are characteristic of EP winters, are unfavorable for winter rainfall in Hawaii. As a result of this robust signal, dry conditions prevail in Hawaii and the standard deviation of rainfall during EP winters is smaller than the climatology. For CP winters, the maximum equatorial ocean warming is weaker and shifted westward to near the date line. The subtropical jet stream retreats westward relative to EP winters and the anomalously sinking motion near Hawaii is variable and generally weaker. Although the anomalous moisture flux divergence still exists over the subtropical North Pacific, its magnitude is weaker relative to EP winters. Without strong external forcing, rainfall in the Hawaiian Islands during CP winters is close to the long-term mean. The spread of rainfall from one CP event to another is also larger. The near-surface minimum temperature from three stations in Hawaii reveals cooling during EP winters and slight warming during CP winters.

KEYWORDS: El Nino; Rainfall; Winter/cool season; Climate variability; Interannual variability

1. Introduction

The Hawaiian Island chain consists of eight major islands, several atolls, and many smaller islets stretching some 2400 km in the subtropical eastern and central North Pacific (Fig. 1). Hawaii is known for its favorable climate and refreshing weather because of its constant temperatures, mild humidity, and breezy trade winds. Persistent northeast trades are important to the Hawaiian Islands because they affect cloud formation and precipitation, wave height, and moderate temperatures. Generally, there are two seasons in Hawaii, with the wet and cool season from November to April, and dry and warm season from May to October.

The rainfall distribution on the Hawaiian Islands is spatially uneven, and the mean rainfall map at the peak wet season is shown in Fig. 2 (Giambelluca et al. 2013). As cumulus cloud clusters associated with the subtropical high pressure in the eastern North Pacific are advected over the Islands, they are forced to rise along with mountain barriers. This uplifting produces orographic clouds and rain along the windward slopes below the trade wind inversion, which acts as a very stable layer that limits cloud growth and turbulent mixing. The trade wind inversion layer in Hawaii is usually found at an elevation of around 2200 m (Cao et al. 2007). As such, the largest amount of mean winter (December–February) rainfall occurs on windward slopes below the inversion layer with a value of approximately 1400 mm season^{-1} over the islands of Hawaii, Maui, Molokai, Oahu, and Kauai (Fig. 2a). On the leeside of the mountains where air sinks and warms, less rainfall occurs (~400 mm season^{-1}). This is known as the rain shadow effect. At the top of Hawaii's highest mountains such as Mauna Loa and Mauna Kea, which are well above 3500 m (Fig. 1), very dry air prevails. For the standard deviation of winter rainfall (Fig. 2b), its pattern is similar to the mean rainfall with large variability (~800 mm season^{-1}) on the eastern mountain slopes of Maui and Hawaii and small spread in the leeward dry areas.

The El Niño–Southern Oscillation (ENSO) phenomenon, the leading mode of tropical climate variability, profoundly modulates Hawaii rainfall. During an El Niño winter and the following spring, droughts tend to occur more often in the Hawaiian Islands (Chu 1989, 1995; Chu and Chen 2005). The opposite is true for La Niña events. In terms of rainfall extremes, more frequent heavy rainfall was observed in Hawaii during La Niña events while there were fewer extreme rainfall events during El Niño (Chu et al. 2010). ENSO exerts its influence on Hawaii through altering atmospheric fields, which are tightly linked to equatorial atmospheric convective heating. For example, enhanced convection and ascending motion are found in the equatorial central Pacific during El Niño winters, giving rise to a strong Hadley type circulation in the central North Pacific. Because Hawaii is located in the sinking branch of this local Hadley cell, low rainfall occurs (Chu 1995; Chu and Chen 2005). Chen and Chu (2014) further examined return levels in rainfall extremes over the last 50 years with respect to ENSO states using a nonstationary generalized extreme value distribution. They found that return levels in Hawaii, i.e., the extreme rainfall rate corresponding to the desired return period (e.g., 100 years), increase during La Niña years and decrease during El Niño years. It should be noted that the relationship between Hawaii winter rainfall and La Niña has been changing and abundant rainfall during La Niña
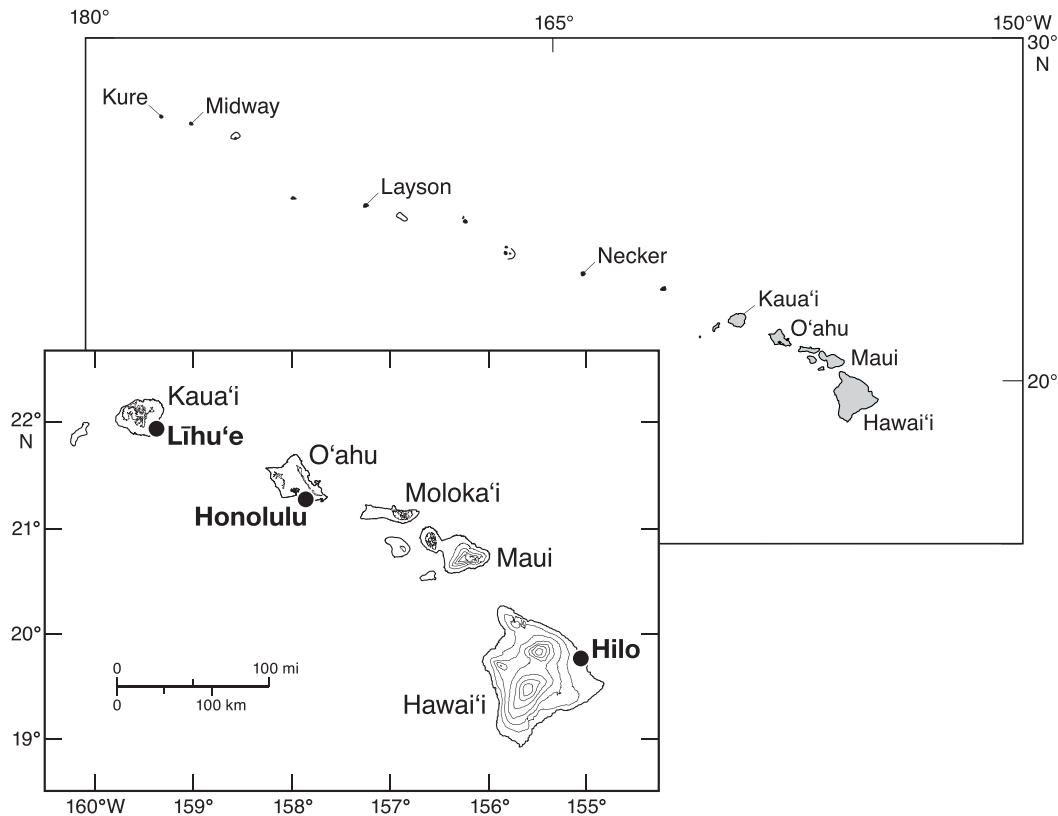
FIG. 1. Orientation map of the Hawaiian Islands. The inset indicates the location of the three stations used (Hilo, Honolulu, and Lihue), and contour interval for elevation is 2000 ft.

is no longer deemed as a certainty. While examining the long-term records from 1956 to 2010, O'Connor et al. (2015) noted a downward shift in La Niña winter rainfall and the turn-around appears to occur in 1983.

El Niño events can be broadly separated into two types or "flavors" (e.g., Ashok et al. 2007; Kao and Yu 2009; Kug et al. 2009): central Pacific (CP) or Modoki events with peak sea surface temperature (SST) anomalies located in the central
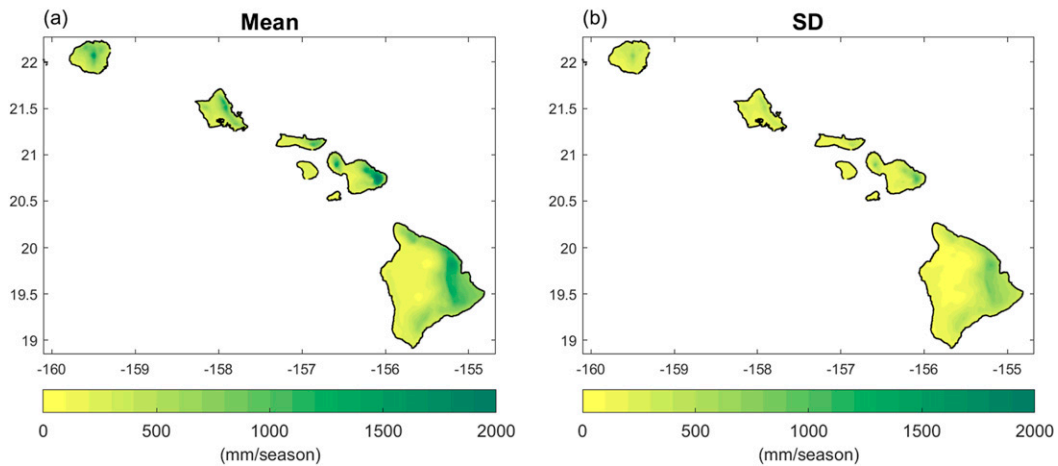

FIG. 2. Climatological rainfall (1971–2000) for (a) seasonal mean (December–February) and (b) standard deviation (SD).

equatorial Pacific, and eastern Pacific (EP) or canonical El Niño events with maximum SST anomaly (SSTA) in the eastern equatorial Pacific. The EP type of El Niño is associated with basinwide thermocline and surface wind variations. The SSTA of this type appears to propagate westward with time. This is in contrast to the CP type, which is characterized by regional variations in ocean temperatures and winds with little indication of the direction of SST propagation (Kao and Yu 2009). In particular, thermocline variations appear to exert less influence on the CP ENSO, and zonal advection and regional air–sea heat fluxes become more important for the central Pacific SSTA (Vimont et al. 2003; Kug et al. 2009; Kao and Yu 2009; Newman et al. 2011).

The zonal advective feedback is manifested by the advection of mean SST gradients by the anomalous eastward mixed layer ocean current associated with the CP El Niño (An and Jin 2001; Kug et al. 2009). The anomalous eastward equatorial ocean current or low-level wind is effective in advecting warm SSTA from the western Pacific to the central Pacific because of the large background zonal SST gradients between the western Pacific warm pool and the eastern Pacific cold tongue. This is different from the EP type where the thermocline-depth displacement is more influential on the eastern Pacific SSTs. Therefore, changes in local SST for the central and eastern Pacific depend on different key dynamical processes. The CP type SSTA may also be generated by atmospheric forcing from the subtropical North Pacific by the seasonal footprinting mechanism (Vimont et al. 2003). The subtropical atmospheric circulation can first induce positive SSTA off Baja California during boreal winter, which then spreads southwestward in the following seasons through the subtropical atmosphere–ocean interaction (i.e., the Pacific meridional mode) and reaches the tropical central Pacific to yield a CP type of El Niño (Kim et al. 2012; Paek et al. 2017). Atmospheric convection anomalies, as inferred from the outgoing longwave radiation, associated with EP and CP events will be presented in section 4.

Previous studies focused on a traditional view of El Niño's effect on Hawaii winter rainfall by lumping all warm events together as a single entity. However, EP and CP El Niño events have distinct impacts on rainfall across the tropical Pacific, with many regions experiencing drier conditions during EP events and wetter conditions during CP events (see Fig. 11; Karamperidou et al. 2015). This study is motivated by the question of whether CP and EP El Niño flavors lead to distinct patterns of rainfall response in the Hawaiian Islands because the maximum SSTA and their attendant convective heating are geographically different. We use three long-term stations with 2-m temperature records in Hawaii to illustrate their relationship with El Niño types. This paper is organized as follows: description of data in section 2; the methodology used in section 3; discussion on rainfall and atmospheric circulation patterns between EP and CP winters, followed by temperature and El Niño types in section 4 and the summary and conclusions in section 5.

2. Data

The National Centers for Environmental Prediction–National Center for Atmospheric Research (NCEP–NCAR)

Reanalysis-1 monthly mean data (Kalnay et al. 1996) with a spatial resolution of 2.5° latitude–longitude for the period of 1950–2019 (70 years) are used in this study. Atmospheric variables include specific humidity, zonal and meridional winds, sea level pressure (SLP), geopotential height, outgoing longwave radiation (OLR), and vertical velocity at the standard vertical levels.

The NOAA extended reconstructed monthly mean SST v4 dataset developed by the NOAA/Earth System Research Laboratory (ESRL) Physical Sciences Division [ERSSTv4; Huang et al. (2015)] with a spatial resolution of 2° latitude–longitude is selected from 1950 to 2019 to determine the ENSO signal. The period of study is selected by consistency with historical El Niño–La Niña episodes (1950–2019) released by NOAA, and the anomalies are computed from a 1971–2000 monthly mean climatology. The Niño-3 (N_3) and Niño-4 (N_4) indices are calculated via monthly mean SSTA over the regions 5°S–5°N and 150°–90°W, and 5°S–5°N and 160°E–150°W, respectively.

The Rainfall Atlas of Hawaii (Giambelluca et al. 2013) is a set of maps of very high spatial distributions of rainfall for major Hawaiian Islands. The monthly mean rainfall data at 250-m resolution, which was updated 1950–2012, is used to represent the regional rainfall climate pattern for the four major Hawaiian Islands (Frazier et al. 2016). Because of the completeness of data between 1950 and 2019, daily surface temperature records, from three airport stations (Honolulu, Lihue, and Hilo) from the National Centers for Environmental Information are selected.

3. Methodology

a. Definition of EP and CP Niño types

Various indices have been proposed to define the two types of El Niño events (e.g., Ashok et al. 2007; Kug et al. 2009; Yeh et al. 2009; Takahashi et al. 2011). For example, an EP (CP) event is identified when the boreal winter N_3 index is greater (smaller) than the corresponding winter N_4 index and the two indices are above 0.5°C. However, the temporal correlation coefficient between N_3 and N_4 is rather high. Because of this high correlation, it is desirable to have a different index to better separate EP from CP events. Ren and Jin (2011) suggest another method to separate these two events using Niño-3 and Niño-4 indices. Their method is described in the following:

$$N_{\mathrm{EP}} = N_3 - aN_4, \qquad (1)$$

$$N_{\mathrm{CP}} = N_4 - aN_3, \qquad (2)$$

where $a = (2/5)$ if $N_3N_4 > 0$ and $a = 0$ if $N_3N_4 \leq 0$.

In Eq. (1), in order to obtain an index for the EP event (N_{EP}), a negative sign is applied in front of N_4 to mitigate the influence of the central Pacific SST variations on the eastern Pacific. This nonlinear transformation works similarly for the N_{CP} index [Eq. (2)]. In Ren and Jin (2011), the transformation coefficient ($a = 0.4$) is determined empirically so that the clusters of EP and CP indices are closer to the center of the new coordinate axes defined by N_{EP} and N_{CP}, while keeping the two

TABLE 1. Years of EP and CP events.

EP year	CP year
1957	1958
1972	1968
1982	1977
1986	1987
1991	1990
1997	1994
2015	2002
	2004
	2006
	2009
	2014
	2018
	2019
Total: 7	Total: 13

indices more or less independent. The CP and EP events are then defined when the monthly mean N_{CP} and N_{EP} is positive and larger than one standard deviation, respectively.

While the method of Ren and Jin (2011) works well for the EP events, there is an issue with the CP events because Eq. (2)

does not consider SST variations over the equatorial western Pacific. Note that SSTA over the equatorial western Pacific is one of the vital components in the construction of the El Niño Modoki index (EMI) in Ashok et al. (2007). To account for the western Pacific SST, the method of Ren and Jin (2011) is modified after running multiple testing as follows:

$$N_{CP}^{*} = N_4 - bN_3 - cN_{weq}, \qquad (3)$$

where $b = 0.37$ if $N_4N_3 > 0$, and $b = 0$ if $N_4N_3 \leq 0$, and $c = 0.49$ if $N_4N_{wea} > 0$, and $c = 0$ if $N_4N_{weq} \leq 0$. The N_{weq} is computed as the spatial mean of the equatorial western Pacific SST (5°S–5°N and 125°–145°E).

After the modification, the correlation coefficient between N_{EP} and N_{CP}^{*} is reduced to 0.29, which is insignificant when taking the persistence of N_{EP} and N_{CP}^{*} into account (e.g., Quenouille 1952; Hastenrath et al. 1984). Moreover, the correlation between the N_{EP} and N_3 is as high as 0.98, signifying that this new index captures the canonical El Niño well. Likewise, the correlation between N_{CP}^{*} and N_4 is 0.86, which means that the new index also mimics and isolates the genuine CP warming episode. The EP and CP events are then defined when the seasonal mean N_{EP} or N_{CP}^{*} between December and
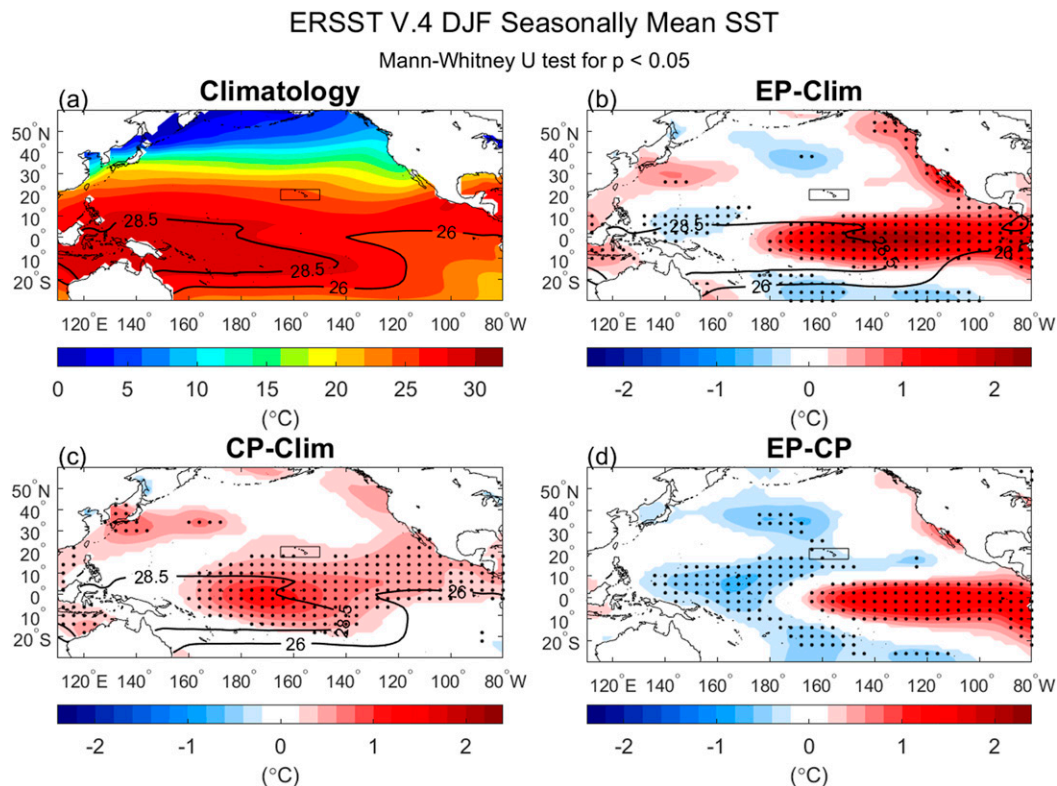

FIG. 3. (a) Climatological mean seasonal (December–February) sea surface temperatures (SST; °C; contours) computed from climatology (1971–2000), (b) anomaly from climatology in EP winters, (c) anomaly from climatology in CP winters, and (d) difference between CP and EP winters. The western Pacific warm pool is defined by the SST above 28.5°C, and the equatorial cold tongue is defined by SSTs less than 26°C. Both regions are denoted by solid lines in (a)–(c). The asterisks in (b)–(d) indicate the grid point where the Wilcoxon–Mann–Whitney rank-sum test is rejected at the 5% level. The Hawaiian Islands are denoted by a rectangular box.
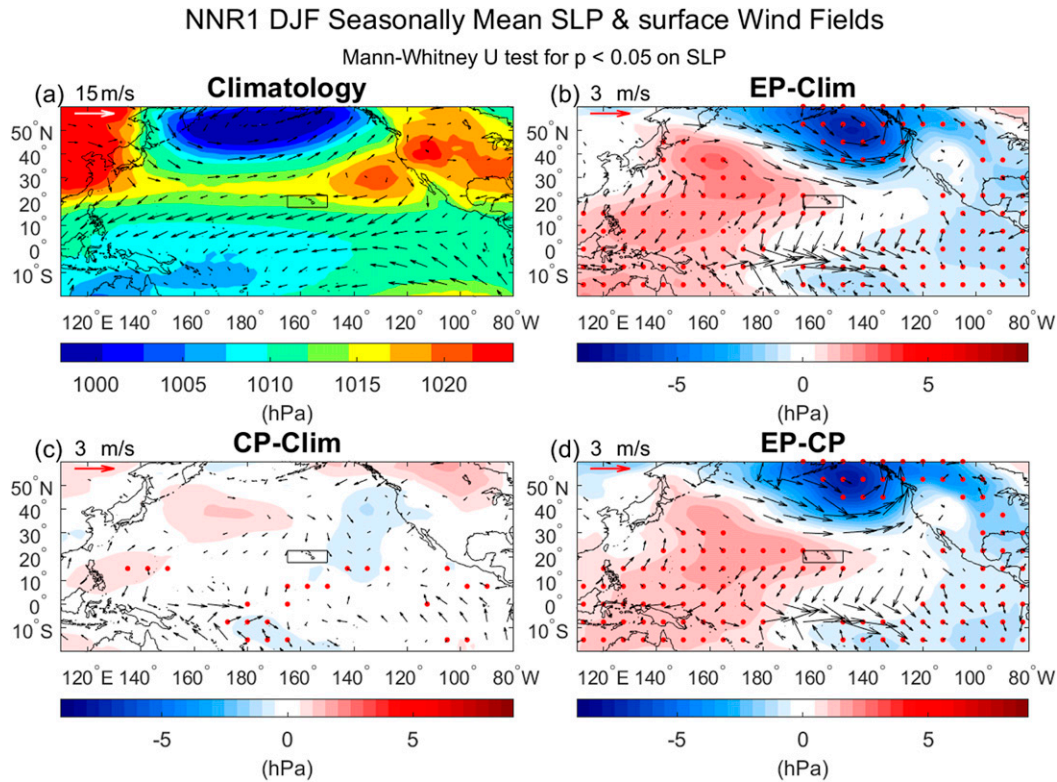
FIG. 4. (a) Climatological mean seasonal (December–February) sea level pressure (shading; hPa) and 10-m wind fields (m s^{-1}) between 60°N and 20°S computed from climatology (1971–2000), (b) anomaly from climatology in EP winters, (c) anomaly from climatology in CP winters, and (d) difference between CP and EP winters. For (b)–(d), positive values are denoted in red and negative values are denoted in blue. The asterisks in (b)–(d) indicate the grid point of SLP where the Wilcoxon–Mann–Whitney rank-sum test is rejected at the 5% level. The Hawaiian Islands are denoted by a rectangular box.

February is positive and larger than one standard deviation away from zero. Using this definition, the events are summarized in Table 1. In all, 7 EP events and 13 CP events are identified. Note the frequent occurrence of CP events since 2000, which is consistent with other studies (e.g., Lee and McPhaden 2010). Specifically, seven CP events have occurred since 2000. In contrast, only one EP event occurred during the same period.

b. Moisture flux convergence

To illustrate the contribution from the amount of moisture and the convergence in the EP and CP winters, a column-integrated moisture transport analysis is performed. The moisture flux convergence (MFC) is composed of the advection and convergence term (Banacos and Schultz 2005; Chu and Chen 2005):

$$\text{MFC} = -\nabla \cdot (q\mathbf{V}_h) = -\mathbf{V}_h \cdot \nabla q - q\nabla \cdot \mathbf{V}_h,$$

$$\text{MFC} = -u\frac{\partial q}{\partial x} - v\frac{\partial q}{\partial y} - q\left(\frac{\partial u}{\partial x} + \frac{\partial v}{\partial y}\right),$$

where q is the specific humidity (g kg^{-1}), $\mathbf{V}_h$ is the horizontal wind fields (m s^{-1}), and ∇ is the horizontal gradient operator.

The contributions from the horizontal disparity of wind speed and moisture on MFC are clearly revealed in the above equation. The vertical integrated MFC is added up from 1000 to 200 hPa in this study. Monthly data from December to February are averaged as the winter (DJF) seasonal mean, and a year is written as December of the first year (e.g., 1982 means from December 1982 to February 1983).

c. Nonparametric Wilcoxon–Mann–Whitney test

A nonparametric Wilcoxon–Mann–Whitney rank-sum test is used to evaluate the difference in location between two data samples. When comparing two different data batches, the common practice is to use a two-sample t test. One of the premises of the t test is that the means of both samples are normally distributed. In this study, because the sample size is small and variables with nonnormal sample distributions are tested (e.g., wind speed, vertical motion), there is no guarantee that the sample means converge to a Gaussian distribution. Accordingly, a classic nonparametric test is used. The null hypothesis is that the two datasets have the same location (i.e., overall magnitude or mean). To perform this test, the two data batches need to be pooled and ranked. For details, see Chu and Chen (2005) and Wilks (2011).

d. Partial correlation and regression

Partial correlations and partial regressions identify the remaining linear relationship between two variables after the influence of a third variable has been controlled, which is useful for discerning the intervening or antecedent role of a variable in a causal link between two other variables (Blalock 1961). To analyze X and Y, given Z as a third variable, the partial correlation is expressed as $r_{XY|Z} = (r_{XY} - r_{XZ}r_{YZ})/\sqrt{(1 - r_{XZ}^2)(1 - r_{YZ}^2)}$. The original Pearson correlation value (r_{XY}) will be influenced if Z is correlated to X and Y. Likewise, partial regression is employed to isolate the impacts of the two independent predictors. Partial regression involves the computation of the linear dependence of a predictand upon a predictor after the linear relationship with a second predictor is controlled from both the predictand and predictor (e.g., Cai et al. 2011).

4. Results

a. Atmospheric circulation in EP versus CP ENSO winters

Figure 3a shows the climatological mean SST (1971–2000, in contours) pattern in boreal winter over the Pacific, from 20°S to 60°N. The presence of the western Pacific warm pool, defined by seasonal mean SST above 28.5°C, and the equatorial cold tongue (SST less than 26°C) in the eastern Pacific are well recognized. During the EP winters, a narrow band of positive SSTA with an east–west extension from the date line to 80°W is observed, with the peak warming of greater than 2°C near 140°W (Fig. 3b). Such an eastward displacement of the warm pool masks the cold tongue in the eastern equatorial Pacific and is statistically significant relative to climatology. Significantly anomalous warming also occurs along the west coast of North America, along with cooling over the central Pacific. In the western Pacific, a dipole pattern of SSTA is seen, with minor cooling near the equator and warming along a strip off the coasts of East Asia.

During CP winters, the area of anomalous warming in the tropical Pacific is also substantial and statistically significant, but the magnitude of warming is weaker and peak SSTA (~1°C) is found near 170°W (Fig. 3c) with a poleward expansion of SSTA. This location of the maximum warming is shifted by 30° longitude westward relative to EP winters. During CP events, the warming off the west coast of North America is insignificant. Note that the Hawaiian Islands experience warmer SSTA during CP winters from the poleward extension of the equatorial central Pacific SSTA. Minor warming is also found near Taiwan and off southern Japan. The difference in SST between the EP and CP (Fig. 3d) is characterized by a large east–west dipole pattern with positive and statistically significant anomalies located along the equator to the east of 160°W, and significant negative anomalies in the western and central equatorial Pacific with extension to the higher latitudes.

Next we examine the climatological mean sea level pressure and 10-m wind patterns, as well as the difference between EP (and CP) and climatology in boreal winter over the Pacific. Climatologically, the Aleutian low pressure system and the subtropical Pacific high, located to the northeast of Hawaii, stand out (Fig. 4a). The subtropical high provides the prevailing northeast trade winds that impact the Hawaiian Islands.
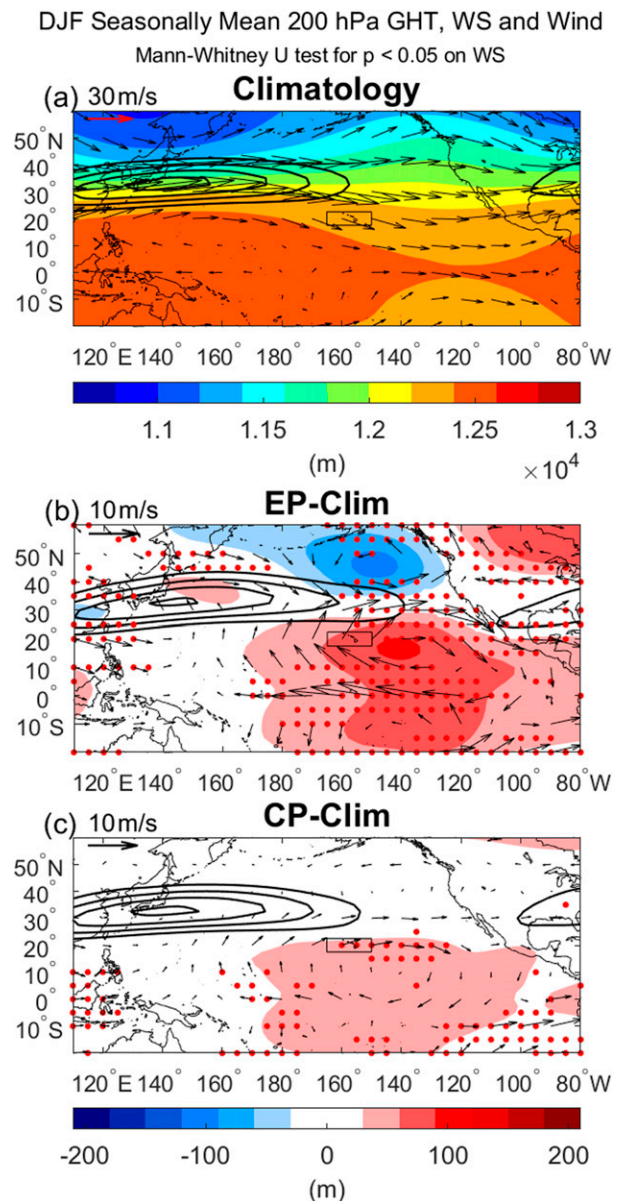

FIG. 5. (a) Climatological mean seasonal (December–February) geopotential height (shading; m), westerly jet stream (contour; m s^{-1}), and wind fields (m s^{-1}) at 200 hPa computed from climatology (1971–2000), (b) anomaly from climatology in EP winters, and (c) anomaly from climatology in CP winters. The westerly jet stream (wind speed > 40 m s^{-1}) is denoted by solid lines in all figures. For (b) and (c), positive values are denoted in red and negative values are denoted in blue. The asterisks in (b) and (c) indicate the grid point of wind speed where the Wilcoxon–Mann–Whitney rank-sum test is rejected at the 5% level.

The Aleutian low deepens significantly and shifts southeastward, which brings anomalously westerly or northwesterly flows to the midlatitude ocean during EP winters (Fig. 4b). Anomalously strong midlatitude westerlies may enhance evaporative cooling and ocean mixing, resulting in cooling of
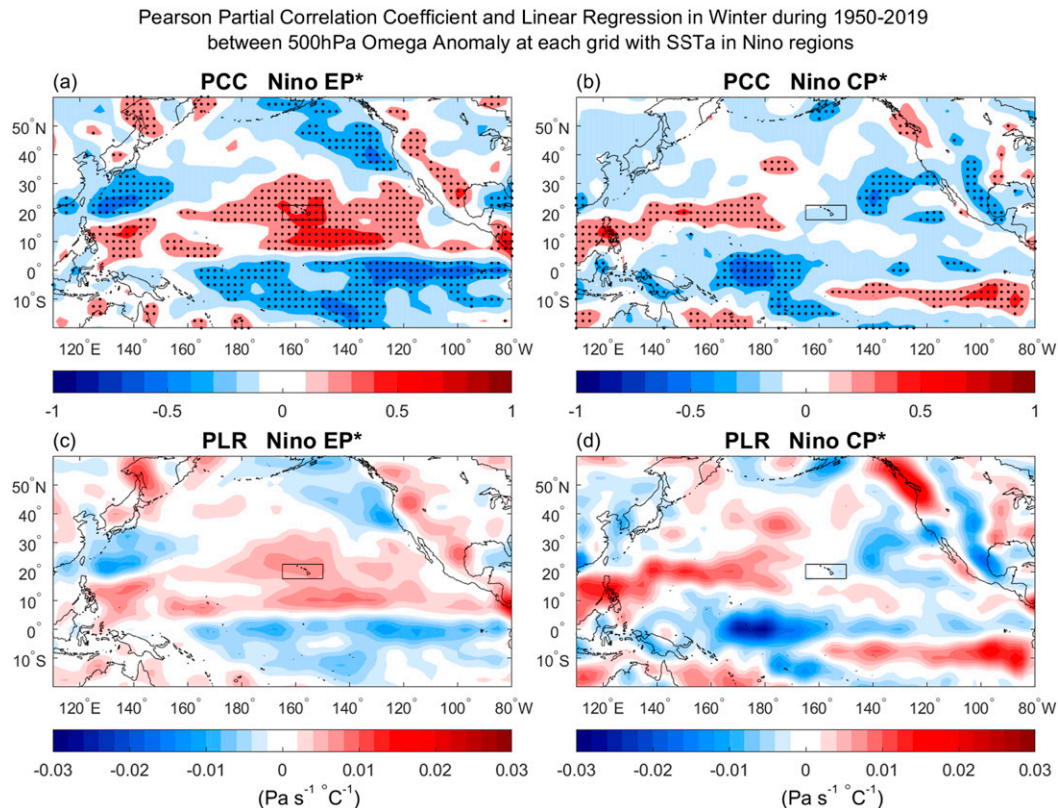
FIG. 6. (a),(b) Partial correlation and (c),(d) partial linear regression (Pa s^{-1} °C^{-1}) between the El Niño indices and anomalous omega at 500 hPa at each grid during boreal winter (DJF) from climatology (1971–2000). Positive (negative) correlation and linear regression are denoted in red (blue). The asterisks in (a) and (b) indicate the grid point where the partial correlation is significant at the 5% level. The Hawaiian Islands are denoted by a rectangular box.

the ocean surface to the north of Hawaii (Fig. 3b). Moreover, westerly or northwesterly anomalies surrounding the Hawaiian Islands would decelerate the trade winds and likely reduce the trade wind–induced orographic rainfall to the islands (Fig. 4b). Trade winds are crucial for rainfall variations in Hawaii (e.g., Lyons 1982; Chu et al. 1993; Timm and Diaz 2009; O'Connor et al. 2015). Diaz and Giambelluca (2012) also found that a deeper Aleutian low and enhancement of the North Pacific surface westerlies are associated with dry winters (November–April) in Hawaii. Southwesterly anomalies on the eastern flank of the enhanced Aleutian low (Fig. 4b) may increase onshore Ekman transport, with the effect of suppressing coastal up-welling off the west coast of North America. This effect aids in the anomalous coastal warming off North America (Fig. 3b). The subtropical high pressure system in the eastern North Pacific weakens during EP winters (Fig. 4b). A synthesis of Figs. 3 and 4 is indicative of dry winters in Hawaii during EP owing to the deepening and southeastward shift of the Aleutian low and attendant low-level North Pacific westerly anomalies, together with the weakening of the subtropical high.

Another signature of the EP El Niño winter evident from Fig. 4b is a positive pressure and anticyclonic anomalies over the Philippines Sea (Wang et al. 2000). Around the eastern flank of the Philippine Sea anticyclone, southward flows, which once crossed the equator, turn to westerlies due to the Coriolis force. A band of equatorial westerly anomalies, resulting from the cross-equatorial flows from both hemispheres, is confined between 150°E and 130°W. Anomalous southwesterly flows on the western side of the Philippines Sea anticyclone transport warmer water to Taiwan and southern Japan (Fig. 3b). The band of northerly anomalies around 10°N in the central Pacific implies a southward shift of the trade wind trough or the in-tertropical convergence zone (ITCZ) in the eastern/central North Pacific during EP winters.

For CP winters (Fig. 4c), the deepening of the Aleutian low is slightly weaker and statistically insignificant but still appears shifted southeastward. The subtropical high in the northeast-ern Pacific is not significantly different from climatology. The band of equatorial westerly anomalies shifts westward during CP winters relative to EP winters (Figs. 4b,c). Figure 4c shows a weak divergence center located to the east of the Philippines.

Next we look at the upper-level circulation associated with two types of El Niño (Fig. 5a). Climatologically during boreal winter, the subtropical jet core, where wind speed exceeds 40 m s^{-1}, extends from East Asia to about 160°W. Higher geo-potential height, related to warm tropospheric temperatures,
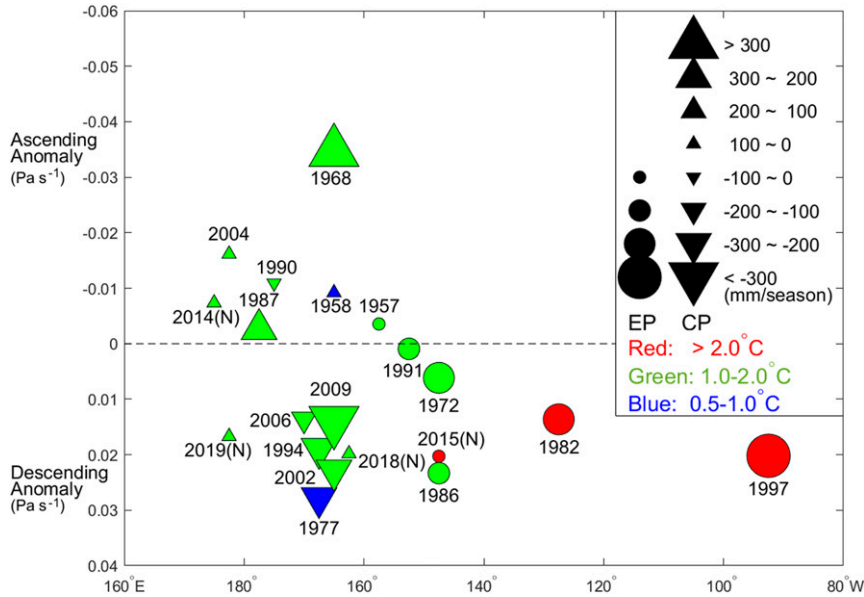
FIG. 7. Scatterplot between the omega anomalies at 500 hPa around the Hawaiian Islands (17.5°–22.5°N, 165°–150°W), the Hawaiian statewide-average rainfall [no rainfall data, as indicated by (N) for 2014, 2015, 2018, and 2019], and the location of maximum equatorial SSTA for each of the individual El Niño winters. Triangles denote CP events and circles for EP events. The size of triangles and circles refers to the amount of rainfall anomalies. The color coding means different magnitudes of SST anomalies.

is found in the tropics and lower height values are observed in the higher latitudes. During EP winters (Fig. 5b), the dominant features are the eastward elongation of the subtropical westerly jet stream over the North Pacific, an extensive area of higher geopotential height in the tropical eastern Pacific, and a pair of anticyclonic circulation anomalies straddling the equator in the central Pacific. The southerly flows in the tropics enhance poleward angular momentum transports, leading to a stronger westerly flow in the northern subtropics. The westerly jet extends eastward to 140°W (Fig. 5b). This is a 20° longitude eastward extension relative to climatology. Hawaii is located near the right exit quadrant of the jet core in an area of upper-level convergence, which is conducive to midtropospheric sinking motion, low-level divergence, and contributes to dry conditions over Hawaii. Other notable features during EP winters (Fig. 5b) are the cyclonic circulation anomaly over the North Pacific and a downstream anticyclonic anomaly over central Canada. This reflects a quasi-stationary Rossby wave train emanating from the upper-tropospheric vorticity source in regions of enhanced tropical convective heating to the extratropics in a great circle trajectory (Horel and Wallace 1981; Hoskins and Karoly 1981).

For CP winters (Fig. 5c), the upper circulation resembles the EP winters (Fig. 5b) but the magnitude of circulation anomalies is much weaker and the pair of the equatorial anticyclonic gyres appears to shift westward relative to EP winters. The westerly jet retreats westward and its leading edge is found near 155°W. As such, Hawaii is no longer located near the right exit quadrant of the jet core. Without strong sinking motion

and low-level divergence, winter rainfall in Hawaii may not be low, as in the case for EP winters.

The previous analysis illustrates the role of vertical motion in Hawaii rainfall during EP and CP event; however, that surmise is qualitatively based on the relative location between the leading edge of the subtropical jet stream and the Hawaiian Islands. How are EP and CP events related to the vertical motion in Hawaii over the last 70 years? Fig. 6 displays the partial correlation and partial linear regression between anomalous omega at 500 hPa and the N_{EP} (N_{CP}^*) after controlling for the N_{CP}^* (N_{EP}) at each grid during boreal winter. The N_{EP} index (Figs. 6a,c) shows a significant positive correlation (i.e., EP El Niño fosters anomalous sinking motion) over a large subtropical-tropical belt, extending from Baja California through the central Pacific to the Philippines. The Hawaiian Islands, in particular, experience a significant positive correlation of 0.42 (Fig. 6a) with a rate of 0.0061 Pa s^{-1}°C^{-1} (Fig. 6c) during EP winters. In the eastern/central equatorial Pacific, an extensive region of negative correlation with a value of −0.5 is found (Fig. 6a). For the N_{CP}^* index, a coherent band of negative correlation from Baja California through Central Pacific to the region of the main equatorial positive SSTA around the date line is found (Fig. 6b). This pattern is in stark contrast to the correlation pattern seen previously during EP winters. In other words, the Hawaiian Islands experience opposite correlations between the Niño index and vertical motion from 0.42 during EP events (Fig. 6a) to −0.07 during CP events (Fig. 6b).

The aforementioned result takes all the N_{EP} or N_{CP}^* time series and calculates their partial correlation with vertical
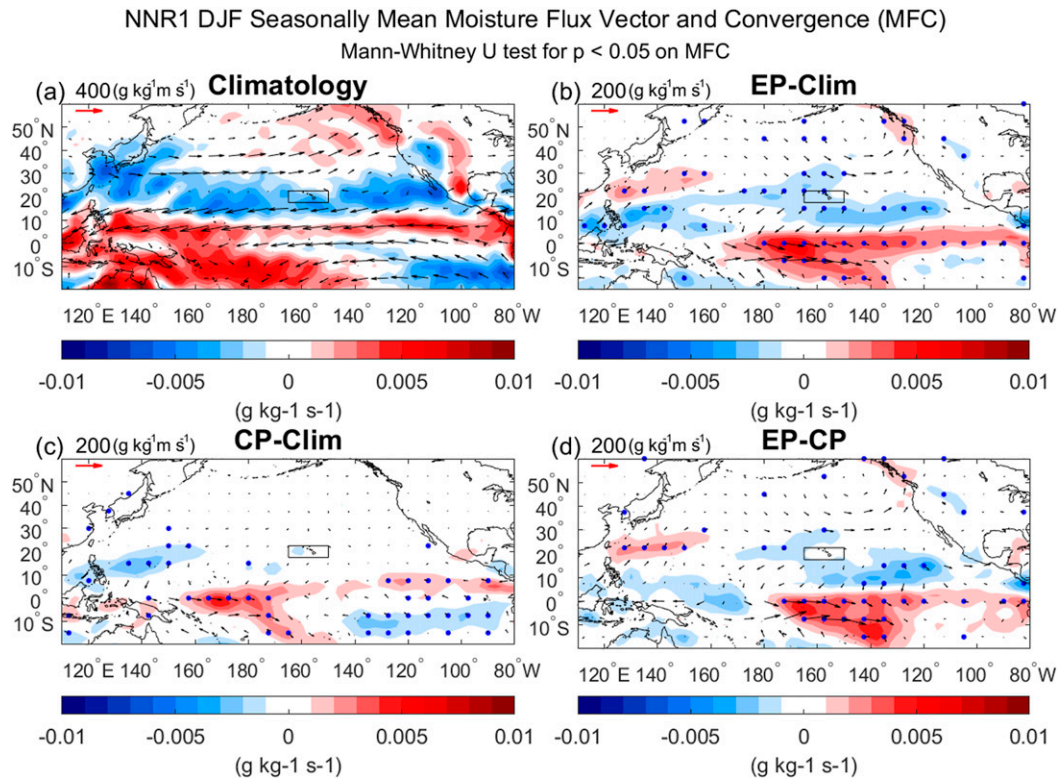
FIG. 8. (a) Climatological mean seasonal (December–February) vertically integrated moisture flux vector $(\mathrm{g\,kg^{-1}\,m\,s^{-1}})$ and convergence (shading; $\mathrm{g\,kg^{-1}\,s^{-1}}$), (b) anomaly from climatology in EP winters, and (c) anomaly from climatology in CP winters, and (d) difference between EP and CP winters. In (a), moisture flux convergence (divergence) is denoted by red (blue). In (b)–(d), anomalous moisture flux convergence (divergence) is denoted in red (blue). The asterisks in (b)–(d) indicate the grid point of MFC where the Wilcoxon–Mann–Whitney rank-sum test is rejected at the 5% level. The Hawaiian Islands are denoted by a rectangular box.

motion. This represents an overall association between an index and vertical motion. Because each El Niño is different, it would also be of interest to investigate the above association for each individual event when the two types of El Niño are considered. Figure 7 is a scatterplot between the omega anomalies at 500 hPa around the Hawaiian Islands (17.5°–22.5°N, 165°–150°W), the Hawaiian statewide-average rainfall, and the longitudes of maximum equatorial SSTA for each El Niño event. There are 20 events in total with 7 EP and 13 CP winters (Table 1). For rainfall, the gridded data are only available up to 2012. Therefore, events after 2012 are not analyzed. As expected, all the EP maximum warmings occurred to the east of 160°W, while CP warming is confined between 170°E and 160°W. Figure 7 has color codes for the magnitude of each Niño event in terms of the equatorial SSTA, and the size of the triangles and circles refers to rainfall anomalies. It is clear that SSTA is generally smaller during CP events relative to EP events. The three strongest EP events are in 1982, 1997, and 2015 (in red).

It is also interesting to note that anomalous sinking motion occurs in six out of seven EP winters and all EP winters are drier (except for 2015 due to lack of rainfall data). This is a rather robust signal because there is an 86% chance for

anomalous sinking motion near Hawaii during an EP El Niño winter in 1950–2019. In addition, all three very strong EP El Niños (1982, 1997, and 2015) are characterized by strong anomalous descending motion. In contrast, six CP winters feature anomalous upward motion and the other seven CP winters reveal anomalous downward motion. Wetter conditions occurred in four of the CP winters and the drier conditions in six CP winters. This result is consistent with Fig. 6b, which shows poor correlation between the N^{*}_{CP} index and vertical motion near Hawaii.

Seasonal mean vertically integrated moisture flux convergence is calculated to identify the flux convergence and divergence regions and their impact on Hawaii winter rainfall. Climatologically, an extensive zonal band of strong moisture convergence near 8°N is found along the ITCZ over the eastern Pacific to the western Pacific warm pool region (Fig. 8a). The north subtropical Pacific, including Hawaii, and the southeastern Pacific are characterized by moisture flux divergence. For EP winters (Fig. 8b), the band of anomalous moisture flux convergence shifts equatorward over the central/eastern Pacific. For CP winters (Fig. 8c), the anomalous pattern mimics the EP winters but the magnitude of change is much smaller (Fig. 8b). It is also of interest to compare moisture flux
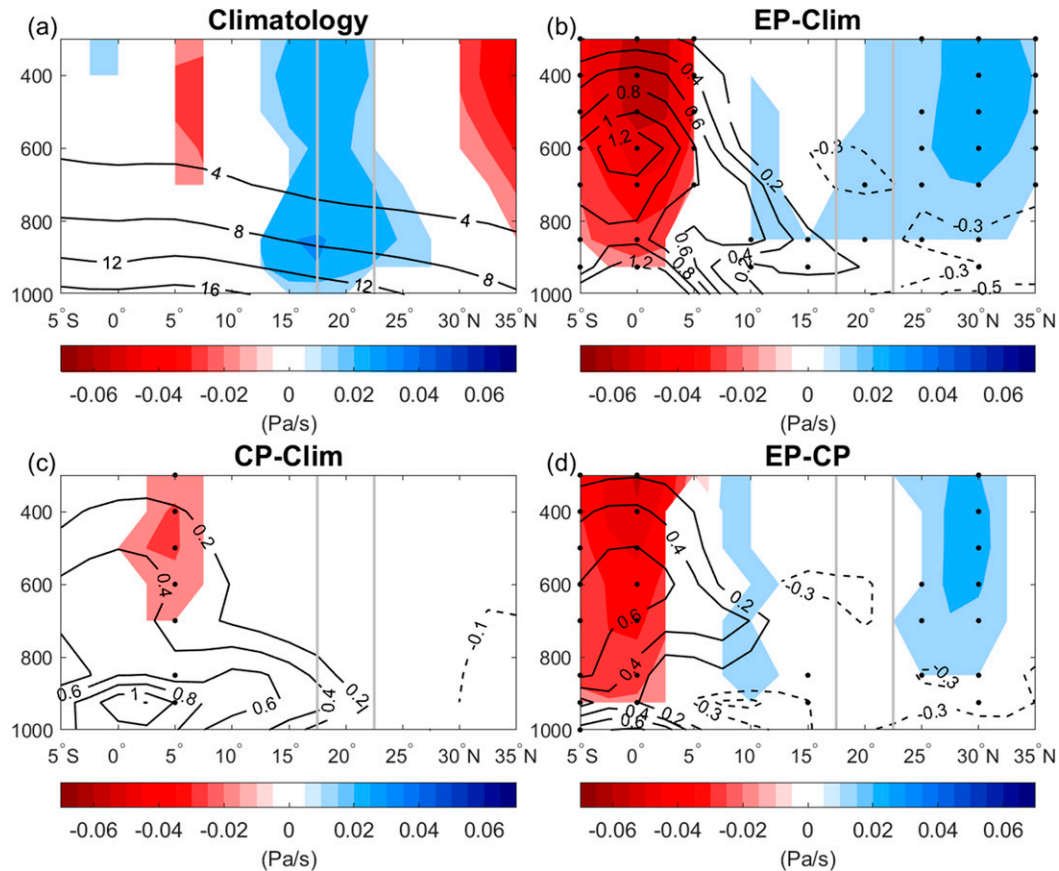
FIG. 9. (a) Climatological mean seasonal (December–February) meridional–vertical circulation. Vertical motion (shading; Pa s^{-1}) and specific humidity (contours; g kg^{-1}) are averaged over 165°–150°W. Ascending motion is in red and descending motion in blue with arrows. (b) Anomaly from climatology in EP winters, (c) anomaly from climatology in CP winters, and (d) difference between CP and EP winters. The Hawaiian Islands are shown by a gray box. In (b)–(d), solid and broken contours denote positive and negative humidity anomalies, respectively. Anomalous ascending (descending) motion is denoted by red (blue) and arrows. The asterisks in (b)–(d) indicate the grid point where the Wilcoxon–Mann–Whitney rank-sum test is rejected at the 5% level.

vectors in the vicinity of Hawaii for these two types of El Niño events. During EP winters (Fig. 8b), the Hawaiian Islands experience much significantly stronger divergence with northwesterly moisture flux anomalies in contrast to insignificant westerly moisture flux anomalies in CP winters (Fig. 8c). It is surmised that the northwesterly flux anomalies during EP winters bring drier and cooler air from the north to the islands.

To highlight the role of the large-scale circulation in Hawaii winter rainfall, the vertical–meridional profile of seasonal mean specific humidity and vertical motion between 165° and 150°W where the Hawaiian Islands are located is depicted in Fig. 9. Climatologically (Fig. 9a), a regional Hadley-type circulation is seen over the central Pacific with ascending motion (red) and higher humidity over the ITCZ and strong descending motion (blue) near the northern subtropics between 12° and 28°N. For EP winters (Fig. 9b), an anomalous sinking motion and lower humidity characterize a very large area between 10° and 35°N over a large portion of the troposphere.

Note that the anomalous sinking motion near Hawaii is statistically significant. Anomalous rising motion and high humidity are located in the equatorial Pacific, where SSTs are abnormally warm (Fig. 3b) and SLPs are abnormally low (Fig. 4b). Compared with EP winters, changes in vertical motion are relatively small, although lower humidity is still observed over the northern subtropics and higher latitudes during CP winters (Fig. 9c). The difference between EP and CP winters reveals anomalous ascending motion (red) near the equator and strong descending motion (blue) between 22° and 35°N (Fig. 9d). As discussed previously, during EP winters wetter and stronger upward motion occurs to the south of 8°N and apparently drier and stronger downward motion dominates the atmosphere around the Hawaiian Islands. Because the main SSTA in CP winters is weaker, the anomalies of moisture and vertical motion are relatively weak and thus close to climatology (Fig. 9c).

In the warm pool region, lower OLR indicates more cloudiness or colder cloud top temperatures, which implies

FIG. 10. (a) Climatological mean seasonal (December–February) outgoing longwave radiation $(\mathrm{W\,m^{-2}})$ at nominal top of atmosphere, (b) anomaly from climatology in EP winters, and (c) anomaly from climatology in CP winters. In (a), more (less) outgoing longwave radiation is denoted by red (blue). For (b)–(d), positive anomalies are denoted in red and negative anomalies in blue. The asterisks in (b)–(d) indicate the grid point of OLR where the Wilcoxon–Mann–Whitney rank-sum test is rejected at the 5% level. The Hawaiian Islands are denoted by a rectangular box.

deeper tropical convection (Fig. 10a). The higher OLR areas are found in the subtropical Pacific and the southeastern Pacific where the SST is low (Fig. 3a). During EP winters (Fig. 10b), significantly higher OLR values (i.e., reduced convection) occur over subtropical eastern North Pacific, including Hawaii, and the western Pacific. Lower and significant OLR values (e.g., enhanced convection) are found in the equatorial central/eastern Pacific, coinciding with the eastward migration of the warm pool during EP winters (Fig. 3b). The dipole pattern in OLR anomalies in the central Pacific also implies the southward shift of ITCZ in EP type. For CP winters (Fig. 10c), changes in OLR values are positive but rather small and insignificant over Hawaii. Overall, reduced convective activity is noted during EP winters but change is small during CP winters over Hawaii.

b. Hawaiian regional climate variability

The spatial anomalous rainfall patterns of seasonal mean and standard deviation (SD) across the Hawaiian Islands between December and February in EP and CP winters from climatology (1971–2000) are illustrated in Fig. 11. Suppressed by the large-scale sinking motion (Fig. 9b), the entire island chain suffers a drier climate during EP winters

(Fig. 11a). Drier conditions are more evident on the windward sides and northern islands as they are closer to the elongated upper-level westerly jet (Fig. 5b), stronger subsidence (Fig. 9b), and weaker trade winds (Fig. 4b). The pattern of changes in the standard deviation during EP winters bears a similar configuration to the corresponding changes in the mean (Fig. 11b). That is, changes in the standard deviation are large (small) in regions where the variation in the mean is large (small). Overall, the variability in rainfall from one EP winter to another is reduced relative to climatology. In other words, the spread of lower rainfall in EP winters becomes small compared to the climatology and is a statewide phenomenon.

In contrast, the change in mean rainfall in CP winters is not obvious. Slightly wetter conditions are shown over low elevations while higher elevations are slightly drier (Fig. 11c). An increase in the standard deviation, which implies more variability in rainfall from one CP winter to another, occurs on the windward side across the islands (Fig. 11d). Corresponding to slightly warmer SST around Hawaii associated with the poleward SSTA from the equator during CP events, weaker moisture flux divergence and the lack of anomalous sinking motion in the vicinity of
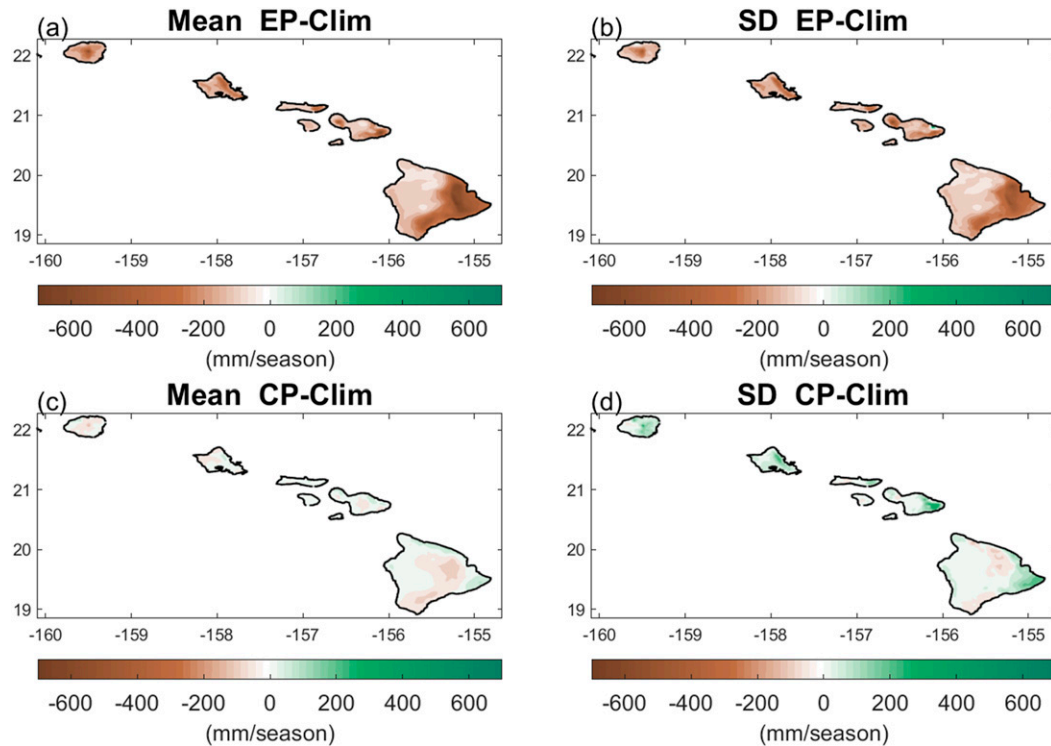
FIG. 11. The top row denotes the (a) anomaly of seasonal mean and (b) anomaly of seasonal standard deviation of rainfall in EP winters. The bottom row denotes the (c) anomaly of seasonal mean and (d) anomaly of seasonal standard deviation of rainfall in CP winters. Unit is mm season^{-1}.

Hawaii (Figs. 8c and 9c) render the rainfall pattern close to the climatology.

Table 2 presents the seasonal mean and standard deviation of precipitation and minimum 2-m temperature anomalies for three stations during two types of El Niño (Fig. 1). In comparison to CP winters, cooler and drier climate with lower standard deviation is observed for the three stations during EP winters. Conversely, slightly warmer conditions with a larger spread in both precipitation and minimum temperature are shown during CP winters relative to EP winters. Note that the differences in both precipitation and minimum temperature composites between the two El Niño types are statistically significant at Hilo and Honolulu. These results are based on station records and are in agreement with the Rainfall Atlas of Hawaii. To further support the impact of El Niño on Hawaiian regional climate variability, Table 3 displays the Pearson correlation coefficients between station rainfall records and key atmospheric variables. A significant correlation of winter rainfall with Niño-3, N_{EP}, and particularly 500-hPa vertical motion is seen, while the response to other Niño indices and local SSTA is weak. Table 4 shows that minimum temperature has a significant correlation with local SSTA and wind speed around Hawaii. As a result, Niño-3 and N_{EP}, and vertical motion are useful diagnostic tools for winter rainfall variations in Hawaii, and minimum temperature is significantly correlated with local SST and wind speed during the winter season.

5. Summary and conclusions

This study investigates the large-scale circulation characteristics of the two types of El Niño (EP and CP) and their impact on Hawaii winter rainfall and temperature using reanalysis and observational data. As expected, the location and amplitude of the maximum SSTA associated with EP and CP El Niño types are different. Relative to the climatology, SST anomalies are more significant and closer to the eastern equatorial Pacific in EP winters, while ocean warming is weaker and near the central Pacific in CP events. Because of this difference and the different amplitudes of anomalous heating, the effect on atmospheric circulation and its impact on regional climate via ENSO teleconnections can vary.

Results demonstrate that during EP winters enhanced moisture flux convergence, stronger upward motion, and active

TABLE 2. Mean (first entry) and standard deviation (second entry) of winter mean precipitation (mm season^{-1}) and minimum temperature (°C) anomaly from climatology (1950–2019) for three stations in Hawaii for two El Niño types.

Mean/SD	$T_{\min}$		Precipitation	
	EP	CP	EP	CP
Honolulu	−0.40/0.70	0.60/0.93	−100/60	−11/170
Lihue	−0.94/0.42	−0.11/1.24	−138/81	−30/235
Hilo	−0.09/0.31	0.41/0.63	−336/167	−28/539

TABLE 3. Pearson correlation coefficient (CC) of seasonal mean precipitation anomaly from climatology (1950–2019) for three stations in two El Niño types. Near-surface wind speed is denoted by WS; Hawaii region is bounded by 18°–24°N and 164°–150°W. Significance test: an asterisk (*) indicates a p value < 0.05 and two asterisks (**) a p value < 0.01.

CC	Niño-3	Niño-4	Niño EP	Niño CP	500-hPa omega Hawaii	SSTA Hawaii	WS Hawaii
Honolulu	−0.32**	−0.20	−0.35**	0.01	−0.80**	−0.01	−0.17
Lihue	−0.35**	−0.28*	−0.35**	−0.09	−0.71**	0.05	−0.02
Hilo	−0.36**	−0.30*	−0.35**	−0.16	−0.38**	−0.15	0.57**

convection are seen over the central and eastern equatorial Pacific. The upper-level anticyclonic anomaly in the tropical central/eastern Pacific associated with strong convective heating accelerates the subtropical jet stream and elongates it eastward over the North Pacific during EP winters. Because the Hawaiian Islands are located in the right exit quadrant of the high-level westerly jet stream, significant descending motion and low-level divergence are expected. At the same time, the Aleutian low deepens and the subtropical Pacific high pressure system slackens. Specifically, midlatitude low-level westerly anomalies enhance ocean mixing and evaporative cooling, leading to cold SSTA to the north of the Hawaiian Islands. These wind anomalies also decelerate the prevailing easterly trade wind speed and result in less trade wind–induced orographic rainfall. Located at roughly 21°N, Hawaii experiences stronger sinking motion resulting from the enhanced local Hadley circulation as well as an eastward elongation of the subtropical jet stream. The sinking motion hinders the development of rain-bearing weather systems such as subtropical cyclones, southward incursions of midlatitude frontal systems, and upper-level disturbances (Chu et al. 1993). As a result, reduced tropical convection and lower rainfall occur in Hawaii during EP winters.

In response to the weaker and westward shift of ocean warming with more northward extension toward the subtropics, changes in atmospheric circulation around the subtropical central North Pacific are less robust during CP winters relative to EP winters. The subtropical central Pacific experiences enhanced descending anomalies and much more stable conditions in EP winters but undergoes warmer SSTA and weaker anomalous descending motion with variable weather in CP winters. For example, the anomalous sinking motion around Hawaii is found in 6 out of 7 EP winters (86%) but occurs in only 7 of 13 CP events (54%). Such a difference in vertical motion also has implications for rainfall variations in Hawaii [100% (6 out of 6) and 60% (6 out of 10) for the drier conditions in EP and CP events, respectively]. While a statewide drought in Hawaii is observed in EP winters, island rainfall during CP winters is not much different from the long-term climatology. Based on

the minimum temperature in three long-term stations in Hawaii (Lihue, Honolulu, and Hilo), we found that cooler and drier climate with small spread dominates during EP winters relative to CP winters. Moreover, the minimum surface temperature in the islands is dependent on the surrounding ocean temperatures and local wind speed during the winter season. The results show that the Niño-3 and N_{EP} indices, and especially the averaged vertical motion surrounding the islands, are useful diagnostic tools for winter rainfall variations in Hawaii.

The results presented in this study may benefit agencies and stakeholders that are concerned with the relationship between El Niño and Hawaii rainfall and temperature. El Niño events have long been perceived as a driver for drought in the State of Hawaii. However, by separating the El Niño events into the EP and CP types, this study reveals that the connection between Hawaii winter rainfall and El Niño is not as straightforward as previously thought. Hawaii winter rainfall during CP events is near the climatological mean value, not necessarily reduced. This new result is a boon for many agencies in Hawaii (e.g., Honolulu Board of Water Supply, the State Department of Land and Natural Resources): a distinction between EP and CP events can prove critical for proper planning and hydrological management.

The climatic hazards of EP El Niño on Hawaii winter rainfall are clearly defined in terms of the large-scale circulation. The circulation features related to CP El Niño and Hawaii rainfall anomalies are less distinct. Currently, we only have a limited understanding of circulation mechanisms associated with the CP–Hawaiian rainfall relationship. For example, why does the anomalous sinking motion near Hawaii occur only 54% of the time during CP events? Background conditions in the extratropics may help explain this variable relationship. For instance, Hawaii rainfall may also be modulated by the Pacific meridional mode (PMM), which is characterized by anomalous warming in the subtropical eastern North Pacific and cooling in the equatorial cold tongue region with strong low-level southwesterly toward the warm lobe (Chiang and Vimont 2004). Because Hawaii is located near the warm lobe of the PMM, more studies are needed to shed light on the role of the

TABLE 4. As in Table 3, but for mean minimum temperature.

CC	Niño-3	Niño- 4	Niño EP	Niño CP	500-hPa omega Hawaii	SSTA Hawaii	WS Hawaii
Honolulu	−0.11	−0.01	−0.13	−0.03	0.16	0.53**	0.33**
Lihue	−0.21	−0.21	−0.18	−0.28*	0.25*	0.25*	0.57**
Hilo	0.07	0.26*	0.02	0.24*	−0.03	0.66**	0.03

PMM and its possible relationship with two types of El Niño in shaping island rainfall.

REFERENCES

An, S. I., and F.-F. Jin, 2001: Collective role of thermocline and zonal advective feedbacks in the ENSO mode. *J. Climate*, **14**, 3421–3432, https://doi.org/10.1175/1520-0442(2001)014<3421:CROTAZ>2.0.CO;2.

Ashok, K., S. K. Behera, S. A. Rao, H. Y. Weng, and T. Yamagata, 2007: El Niño Modoki and its possible teleconnection. *J. Geophys. Res.*, **112**, C11007, https://doi.org/10.1029/2006JC003798.

Banacos, P. C., and D. M. Schultz, 2005: The use of moisture flux convergence in forecasting convective initiation: Historical and operational perspectives. *Wea. Forecasting*, **20**, 351–366, https://doi.org/10.1175/WAF858.1.

Blalock, H., 1961: *Causal Inferences in Nonexperimental Research.* The University of North Carolina Press, 193 pp.

Cai, W., P. van Rensch, T. Cowan, and H. H. Hendon, 2011: Teleconnection pathways of ENSO and the IOD and the mechanisms for impacts on Australian rainfall. *J. Climate*, **24**, 3910–3923, https://doi.org/10.1175/2011JCLI4129.1.

Cao, G., T. W. Giambelluca, D. E. Stevens, and T. A. Schroeder, 2007: Inversion variability in the Hawaiian trade wind regime. *J. Climate*, **20**, 1145–1160, https://doi.org/10.1175/JCLI4033.1.

Chen, Y. R., and P.-S. Chu, 2014: Trends in precipitation extremes and return levels in the Hawaiian Islands under a changing climate. *Int. J. Climatol.*, **34**, 3913–3925, https://doi.org/10.1002/joc.3950.

Chiang, J. C., and D. J. Vimont, 2004: Analogous Pacific and Atlantic meridional modes of tropical atmosphere–ocean variability. *J. Climate*, **17**, 4143–4158, https://doi.org/10.1175/JCLI4953.1.

Chu, P.-S., 1989: Hawaiian drought and Southern Oscillation. *Int. J. Climatol.*, **9**, 619–631, https://doi.org/10.1002/joc.3370090606.

——, 1995: Hawaii rainfall anomalies and El Niño. *J. Climate*, **8**, 1697–1703, https://doi.org/10.1175/1520-0442(1995)008<1697:HRAAEN>2.0.CO;2.

——, and H. Chen, 2005: Interannual and interdecadal rainfall variations in the Hawaiian Islands. *J. Climate*, **18**, 4796–4813, https://doi.org/10.1175/JCLI3578.1.

——, A. J. Nash, and F. Porter, 1993: Diagnostic studies of two contrasting rainfall episodes in Hawaii: Dry 1981 and wet 1982. *J. Climate*, **6**, 1457–1462, https://doi.org/10.1175/1520-0442(1993)006<1457:DSOTCR>2.0.CO;2.

——, Y. R. Chen, and T. A. Schroeder, 2010: Changes in precipitation extremes in the Hawaiian Islands in a warming climate. *J. Climate*, **23**, 4881–4900, https://doi.org/10.1175/2010JCLI3484.1.

Diaz, H. F., and T. W. Giambelluca, 2012: Changes in atmospheric circulation patterns associated with high and low rainfall regimes in the Hawaiian Islands region on multiple time scales. *Global Planet. Change*, **98–99**, 97–108, https://doi.org/10.1016/j.gloplacha.2012.08.011.

Frazier, A. G., T. W. Giambelluca, H. F. Diaz, and H. L. Needham, 2016: Comparison of geostatistical approaches to spatially interpolate month-year rainfall for the Hawaiian Islands. *Int. J. Climatol.*, **36**, 1459–1470, https://doi.org/10.1002/joc.4437.

Giambelluca, T. W., Q. Chen, A. G. Frazier, J. P. Price, Y. Chen, P.-S. Chu, J. K. Eischeid, and D. M. Delparte, 2013: Online rainfall Atlas of Hawai'i. *Bull. Amer. Meteor. Soc.*, **94**, 313–316, https://doi.org/10.1175/BAMS-D-11-00228.1.

Hastenrath, S., M.-C. Wu, and P.-S. Chu, 1984: Towards the monitoring and prediction of northeast Brazil drought. *Quart. J. Roy. Meteor. Soc.*, **110**, 411–425, https://doi.org/10.1002/qj.49711046407.

Horel, J. D., and J. M. Wallace, 1981: Planetary-scale atmospheric phenomena associated with the Southern Oscillation. *Mon. Wea. Rev.*, **109**, 813–829, https://doi.org/10.1175/1520-0493(1981)109<0813:PSAPAW>2.0.CO;2.

Hoskins, B. J., and D. J. Karoly, 1981: The steady linear response of a spherical atmosphere to thermal and orographic forcing. *J. Atmos. Sci.*, **38**, 1179–1196, https://doi.org/10.1175/1520-0469(1981)038<1179:TSLROA>2.0.CO;2.

Huang, B., and Coauthors, 2015: Extended reconstructed sea surface temperature version 4 (ERSST.v4). Part I: Upgrades and intercomparisons. *J. Climate*, **28**, 911–930, https://doi.org/10.1175/JCLI-D-14-00006.1.

Kalnay, E., and Coauthors, 1996: The NCEP/NCAR 40-Year Reanalysis Project. *Bull. Amer. Meteor. Soc.*, **77**, 437–472, https://doi.org/10.1175/1520-0477(1996)077<0437:TNYRP>2.0.CO;2.

Kao, H., and J. Yu, 2009: Contrasting eastern-Pacific and central-Pacific types of ENSO. *J. Climate*, **22**, 615–632, https://doi.org/10.1175/2008JCLI2309.1.

Karamperidou, C., P. N. Di Nezio, A. Timmermann, F.-F. Jin, and K. M. Cobb, 2015: The response of ENSO flavors to mid-Holocene climate: Implications for proxy interpretation. *Paleoceanography*, **30**, 527–547, https://doi.org/10.1002/2014PA002742.

Kim, S. T., J. Yu, A. Kumar, and H. Wang, 2012: Examination of the two types of ENSO in the NCEP CFS model and its extratropical associations. *Mon. Wea. Rev.*, **140**, 1908–1923, https://doi.org/10.1175/MWR-D-11-00300.1.

Kug, J., F. Jin, and S. An, 2009: Two types of El Niño events: Cold tongue El Niño and warm pool El Niño. *J. Climate*, **22**, 1499–1515, https://doi.org/10.1175/2008JCLI2624.1.

Lee, T., and M. J. McPhaden, 2010: Increasing intensity of El Niño in the central-equatorial Pacific. *Geophys. Res. Lett.*, **37**, L14603, https://doi.org/10.1029/2010GL044007.

Lyons, S. W., 1982: Empirical orthogonal function analysis of Hawaiian rainfall. *J. Appl. Meteor.*, **21**, 1713–1729, https://doi.org/10.1175/1520-0450(1982)021<1713:EOFAOH>2.0.CO;2.

Newman, M., S.-I. Shin, and M. A. Alexander, 2011: Natural variation in ENSO flavors. *Geophys. Res. Lett.*, **38**, L14705, https://doi.org/10.1029/2011GL047658.

O'Connor, C. F., P.-S. Chu, P. Hsu, and K. Kodama, 2015: Variability of Hawaiian winter rainfall during La Niña events since 1956. *J. Climate*, **28**, 7809–7823, https://doi.org/10.1175/JCLI-D-14-00638.1.

Paek, H., J.-Y. Yu, and C. Qian, 2017: Why were the 2015-2016 and 1997-1998 extreme El Niños different? *Geophys. Res. Lett.*, **44**, 1848–1856, https://doi.org/10.1002/2016GL071515.

Quenouille, M. H., 1952: *Associated Measurements.* Butterworth Scientific Publications, 242 pp.

Ren, H.-L., and F.-F. Jin, 2011: Niño indices for two types of ENSO. *Geophys. Res. Lett.*, **38**, L04704, https://doi.org/10.1029/2010GL046031.

Takahashi, K., A. Montecinos, K. Goubanova, and B. Dewitte, 2011: ENSO regimes: Reinterpreting the canonical and Modoki El Niño. *Geophys. Res. Lett.*, **38**, L10704, https://doi.org/10.1029/2011GL047364.

Timm, O., and H. F. Diaz, 2009: Synoptic-statistical approach to regional downscaling of IPCC twenty-first-century climate projection: Seasonal rainfall over the Hawaiian Islands. *J. Climate*, **22**, 4261–4280, https://doi.org/10.1175/2009JCLI2833.1.

Vimont, D. J., J. M. Wallace, and D. S. Battisti, 2003: The seasonal footprinting mechanism in the Pacific: Implications for ENSO.

J. Climate, **16**, 2668–2675, https://doi.org/10.1175/1520-0442(2003)016<2668:TSFMIT>2.0.CO;2.

Wang, B., R. Wu, and X. Fu, 2000: Pacific–East Asian teleconnection: How does ENSO affect East Asian climate? *J. Climate*, **13**, 1517–1536, https://doi.org/10.1175/1520-0442(2000)013<1517:PEATHD>2.0.CO;2.

Wilks, D. S., 2011: *Statistical Methods in the Atmospheric Sciences*. 3rd ed. International Geophysics Series, Vol. 100, Academic Press, 704 pp.

Yeh, S. H., J. S. Kug, B. Dewitte, M. H. Kwon, B. P. Kirtman, and F. F. Jin, 2009: El Niño in a changing climate. *Nature*, **461**, 511–514, https://doi.org/10.1038/nature08316.